Strong interplay between electron-phonon interaction and disorder in low-doped systems

Domenico Di Sante[1,2,*] and Sergio Ciuchi[1,3,4,†]
[1]*University of L'Aquila, Department of Physical and Chemical Sciences, Via Vetoio, L'Aquila, Italy*
[2]*CNR-SPIN, Via Vetoio, L'Aquila, Italy*
[3]*CNISM, Udr L'Aquila, Italy*
[4]*CNR-ISC, Via dei Taurini, Rome, Italy*
(Received 2 May 2014; revised manuscript received 22 July 2014; published 8 August 2014)

The effects of doping on the spectral properties of low-doped systems are investigated by means of the coherent potential approximation to describe the distributed disorder induced by the impurities and the phonon-phonon noncrossing approximation to characterize a wide class of electron-phonon interactions that dominate the low-energy spectral features. When disorder and electron-phonon interaction work on comparable energy scales, a strong interplay between them arises, the effect of disorder can no longer be described as a mere broadening of the spectral features, and the phonon signatures are still visible despite the presence of strong disorder. As a consequence, the disorder-induced metal-insulator transition is strongly affected by a weak or moderate electron-phonon coupling, which is found to stabilize the insulating phase.

DOI: 10.1103/PhysRevB.90.075111 PACS number(s): 63.20.kd, 73.20.Hb, 74.25.Jb

I. INTRODUCTION

In the past years, the development of more accurate methods of investigations, such as angular resolved photoemission spectroscopy (ARPES), combined with the fabrication of novel materials such as high-T_c superconductors [1,2], colossal magnetoresistance manganites [3], correlated oxides [4], topological insulators [5], and graphene [6] in different topological conditions (from bulk, to surfaces and heterostructures, up to single monolayers), has enabled us to gain a deep insight into low-energy electronic and spectral properties. The continuously increased measurement accuracy in experiments gives us the opportunity to detect and study such low-energy features, which in many cases were recognized as the fingerprint of the electron-phonon interaction.

The possibility to tune the chemical potential by doping offers a great potentially useful way to modify the materials' electronic structures and properties. Very recently, in low doping conditions, electron-phonon signatures were successfully detected in the ARPES spectra of many different systems, from an oxygen vacancies doped $SrTiO_3$ surface [7] or lightly bulk doped $SrTiO_3$ [8,9], to monolayer pnictide FeSe growth on $SrTiO_3$ [10], from tridimensional anatase [11] to $Ba_{1-x}K_xBiO_3$ [12] and $Cu_xBi_2Se_3$ [13] superconductors, up to Z_2 topologically nontrivial materials such as Bi_2Se_3 and Bi_2Te_3 [13], as well as on quasi-two-dimensional layered lightly doped Sr_2TiO_4 [14]. Such a rich variety of different materials displaying common electron-phonon low-energy features calls for a deeper understanding of the underlying mechanism at play. However, once all these systems are taken into account, and in particular when dealing with surfaces, monolayers, and low-dimensional systems, the role of disorder cannot be neglected. In fact, the growth processes on substrates and/or the action of chemical doping imply the presence of disorder, whose impact depends largely on which energy scale one is focused on. For example, impurity bands can be formed close to the conduction band of the pristine material as a consequence of the presence of the dopant energy levels [14,15], or they can have magnetic origins as in Mn-doped GaAs [16,17]. On the other hand, oxygen vacancies on the substrate [7] may represent centers of scatterings for carriers in the deposited film. Interestingly, in this sense, recent ARPES experiments and *ab initio* theoretical works suggested how charge carriers can be trapped by oxygen vacancies at the $LaAlO_3/SrTiO_3$ (LAO/STO) interface [18] and the $SrTiO_3$ surface [19,20], naturally introducing the role of disorder in the understanding of the electronic properties of oxide-oxide heterostructure interfaces and oxide surfaces, where confined two-dimensional electron gases (2DEGs) should also undergo superconducting phase transitions [21].

Usually disorder can be added perturbatively in the theoretical explanation of ARPES spectra as a weak source of scattering leading to an intrinsic band linewidth. Within this approach, interactions such as electron-phonon coupling contribute to the low-energy properties of the spectrum, and the disorder simply provides a further smearing of the electron-phonon features. However, this is not the case when disorder and electron-phonon interaction act on comparable energy scales. For example, let us consider the case of an intermediate electron-phonon coupling; in the very low doping limit, the system is prone to polaron formation, and the presence of scattering centers may provide, in a synergic way, the necessary energy to localize a small polaron [22–26]. Another example is that of a low (but finite) electron density and weak electron-phonon coupling. In this case, when disorder and electron-phonon interaction are treated self-consistently, impurity and phonon contributions to electron scattering are not additive when the Fermi energy is of the order of the phonon frequency [27,28], and impurity scattering has a significant nonlinear effect [29]. In this work, we approach the problem of the interplay between disorder and electron-phonon interaction starting from a weak electron-phonon coupling, going beyond the self-consistent Born approximation used in Refs. [27–29] by using the coherent potential approximation (CPA), thus extending our treatment to the case of strong disorder. Previous studies of models in this peculiar regime concentrated on

*domenico.disante@aquila.infn.it
†sergio.ciuchi@aquila.infn.it

the case of classical phonons in binary alloys [30] or, in the same context, on the effects of electron-phonon interaction on transport properties at high temperature [31]. Electron-phonon interaction and strong disorder have also been studied in the classical phonon case [32] within the context of the Falicov-Kimball model of correlated electrons, for which the CPA is the exact solution [33]. Noticeably, the Mott transition in the Falicov-Kimball model can be described as a disorder-induced metal-insulator transition (MIT) in the alloy context [33]. Here we address the single-particle properties, namely how disorder and electron-phonon interaction modifies ARPES spectra of lightly doped materials [34]. A proper quantum treatment of the phonon is, in this case, crucial to explain the low-energy features of ARPES spectra. The disorder-induced metal-insulator transition is also studied as it depends on the strength of the electron-phonon interaction.

The paper is organized as follows: In Sec. II, we discuss the model Hamiltonians and the types of electron-phonon couplings taken into account in this work. In Sec. III, we explain how such models can be solved in the presence of local disorder as introduced by an Anderson-type Hamiltonian, and we discuss the fluctuation of the electron-phonon self-energy due to disorder. In Sec. IV, we present the main results of our work, discussing the interplay between electron-phonon interaction and disorder to explain the features of the ARPES spectra. We discuss also the electron-phonon dependence of the disorder-induced metal-insulator transition. In Sec. V, we draw our conclusions and make some additional remarks.

II. MODEL HAMILTONIANS

We consider in this work an Anderson-type Hamiltonian for two-dimensional tight-binding electrons interacting with dispersionless optical phonon modes of the general form

$$H = H_{\rm el} + H_{\rm ph} + H_{e\text{-ph}} + H_{\rm dis}. \tag{1}$$

The electronic nearest-neighbor tight-binding part $H_{\rm el} = -t\sum_{\langle i,j\rangle}(c_i^\dagger c_j + \text{H.c.})$ gives rise to a two-dimensional energy dispersion $\varepsilon_k = -2t(\cos k_x + \cos k_y)$; $c_i^\dagger$ and c_i are the charge carrier creation and annihilation operators, respectively. The half-bandwidth $D = 4t$ will be the energy unit throughout the paper, and all k-vectors are given in units of π/a, where a is the lattice spacing. We also choose the zero energy level $\omega = 0$ to the position of the chemical potential.

The disorder part is assumed to be of the Anderson type,

$$H_{\rm dis} = \sum_i \xi_i c_i^\dagger c_i, \tag{2}$$

where ξ_i are disorder-independent random energies taken according to the following disorder distributions:

(i) The bimodal $P_i(\xi) = x\delta(\xi - E_b) + (1-x)\delta(\xi)$ characterizing a concentration of x impurities in the host material.

(ii) The Gaussian $P_g(\xi) = (1/\sqrt{2\sigma^2})\exp(-\xi^2/2\sigma^2)$, where σ^2 is the disorder variance to mimic a conformational disorder.

(iii) As the sum of two independent variables, one of which distributed according to P_i, and the other one distributed according to P_g.

For the free-phonon part, we assume a simple undispersed Einstein phonon Hamiltonian $H_{\rm ph} = \omega_0 \sum_i a_i^\dagger a_i$ with a characteristic phonon frequency ω_0. We fix the value of the phonon frequency in the adiabatic regime $\omega_0/D = 0.05$.

For the electron-phonon interaction part $H_{e\text{-ph}}$, we consider three different kinds of models. The first two can be obtained from the following density-displacement Hamiltonian:

$$H_{e\text{-ph}} = -\sum_{i,j} g_{i,j} c_i^\dagger c_i (a_j + a_j^\dagger). \tag{3}$$

The Holstein local (LOC) model is obtained when $g_{i,j} = g\delta_{i,j}$, whereas a general, even long-range, Fröhlich-type interaction (NLOC) can be considered in more general cases. In the spirit of our work, we focus our attention here on the two-dimensional screened Fröhlich-type interaction. Let us consider the long-wavelength limit of the Fourier transform of the longitudinal-optic (LO) polar coupling $[g^2]_{i,j} = \sum_k g_{i,k} g_{k,j}$,

$$g^2(\mathbf{k}) = \frac{1}{N}\sum_R e^{-i\mathbf{k}\cdot\mathbf{R}}[g^2]_{i,i+R}. \tag{4}$$

If $g^2(\mathbf{k})$ is of the Fröhlich type, i.e., $g^2(\mathbf{k}) \propto 1/k^2$, after summing over all possible values of k_z, we get an effective coupling that at small k behaves as $g^2(\mathbf{k}) \propto 1/k$ depending only on the two-dimensional wave vector $\mathbf{k}$ [35]. Since in our model electrons are free to have planar motions, we next consider the action of the two-dimensional screening of the in-plane carriers. This screening is independent of the carrier density, and the effective coupling is thus replaced by $g^2(\mathbf{k}) \to g^2(\mathbf{k})/\epsilon(\mathbf{k},\omega = 0)$, where $\epsilon(\mathbf{k},\omega = 0) = 1 + \kappa/k$ and $\kappa = 2m^* e^2/\hbar^2\epsilon_r$ is the two-dimensional screening wave vector. The large-k behavior of $g^2(\mathbf{k})$ is obtained restoring the lattice symmetries by replicating the small-k form

$$g^2(\mathbf{k}) = \frac{C}{N_{\mathbf{G}}}\sum_{\mathbf{G}} \frac{|\mathbf{k}+\mathbf{G}|}{|\mathbf{k}+\mathbf{G}| + \kappa}, \tag{5}$$

where $\mathbf{G}$ is a reciprocal-lattice vector and $N_{\mathbf{G}}$ is the number of summed terms in Eq. (5). For our aims, we find that a summation over the nearest-neighbor reciprocal vectors is sufficient. The normalization constant C is chosen by fixing the value of a coupling constant g,

$$g^2 = \frac{1}{N}\sum_{\mathbf{k}} g^2(\mathbf{k}). \tag{6}$$

In both LOC and NLOC models, the dimensionless electron-phonon coupling constant is defined in terms of g as [36]

$$\lambda = 2g^2/\omega_0 D. \tag{7}$$

Another model that we consider in this work is the so-called interaction with a phonon mode such as that occurring with apical oxygens in layered perovskites [37], which we refer to hereafter as the apical oxygens Hamiltonian (AO) [38]. The form of the Hamiltonian is the same as in Eq. (1), but now we consider several two-dimensional planes where electron carriers are free to move (index α) unconnected by out-of-plane hopping processes. The interaction between different planes is introduced through the following AO electron-phonon

coupling:

$$H_{e\text{-ph}}^{\text{BM}} = -\frac{g}{\sqrt{2}} \sum_{i,\alpha} c_{i,\alpha}^{\dagger} c_{i,\alpha} (x_{i,\alpha+1/2} - x_{i,\alpha-1/2}), \tag{8}$$

where $x_{i,\alpha+1/2}$ is the (dimensionless) displacement $x_{i,\alpha+1/2} = (a_{i,\alpha+1/2}^{\dagger} + a_{i,\alpha+1/2})$ of the interplane apical atom in the ith site of the αth plane. Within this AO model, disorder variables are chosen uncorrelated as before, and the Anderson term now reads $H_{\text{dis}}^{\text{BM}} = \sum_{i,\alpha} \xi_{i,\alpha} c_{i,\alpha}^{\dagger} c_{i,\alpha}$. In the AO model, the dimensionless electron-phonon coupling constant is defined as in the LOC and NLOC models through Eq. (7).

III. METHODS OF SOLUTION FOR LOCAL AND NONLOCAL ELECTRON-PHONON HAMILTONIANS

A. The CPA and the phonon-phonon noncrossing approximation in the Holstein model

Here we introduce our approximations in the case of purely local electron-phonon interaction (LOC). We use the CPA to treat the local disorder. The CPA can be thought of as an exact theory on an infinite coordination lattice [39]; for this reason, it is therefore very similar to the single-site dynamical mean-field theory (DMFT) [40,41]. As in DMFT, to solve the LOC model we consider a single site embedded into a self-consistent medium [41]. The single-site propagator $\mathcal{G}$ can be expressed in terms of a local propagator which embodies the *average* action of the environment $[G_0(\omega)]$ and a self-energy $\Sigma(\omega)$ [41]:

$$\mathcal{G}(\omega) = \frac{1}{G_0^{-1}(\omega) - \Sigma(\omega)}. \tag{9}$$

The site propagator $\mathcal{G}$ can be expressed as an average over disorder variable (hereafter a generic quantity A that depends on disorder realizations is denoted by $\hat{A}$, while its average is $A = [\hat{A}]_{\xi}$),

$$\mathcal{G}(\omega) = \left[\frac{1}{G_0^{-1}(\omega) - \xi - \hat{\Sigma}_{e\text{-ph}}(\omega)} \right]_{\xi}, \tag{10}$$

where ξ is the local disorder variable and $\hat{\Sigma}^{e\text{-ph}}(\omega)$ is the electron-phonon self-energy, which depends on the local disorder variables.

Electron-phonon interaction in the LOC model can be self-consistently taken into account within a CPA—or equivalently DMFT—scheme at zero electron density [42]. At finite electron density, we choose a self-consistent phonon-phonon noncrossing approximation (PPNCA) for the electron-phonon self-energy [43] [see the diagrams of type (a) in Fig. 1]:

$$\hat{\Sigma}_{e\text{-ph}}(\omega) = -\frac{g^2}{\beta} \sum_{m} D^0(\omega - \imath\omega_m) \hat{\mathcal{G}}(\imath\omega_m) + \hat{\Sigma}_H, \tag{11}$$

where $D^0(\omega)$ is the free-phonon Green's function while the frequency-independent Hartree term of the electron-phonon self-energy,

$$\hat{\Sigma}_H = -\frac{2g^2}{\omega_0} \hat{n}, \tag{12}$$

is expressed in term of the local density $\hat{n}$, which is given by $\hat{n} = \frac{1}{\beta} \sum_n \hat{\mathcal{G}}(\imath\omega_n) e^{i\omega_n 0^+}$. In this approximation, the phonon

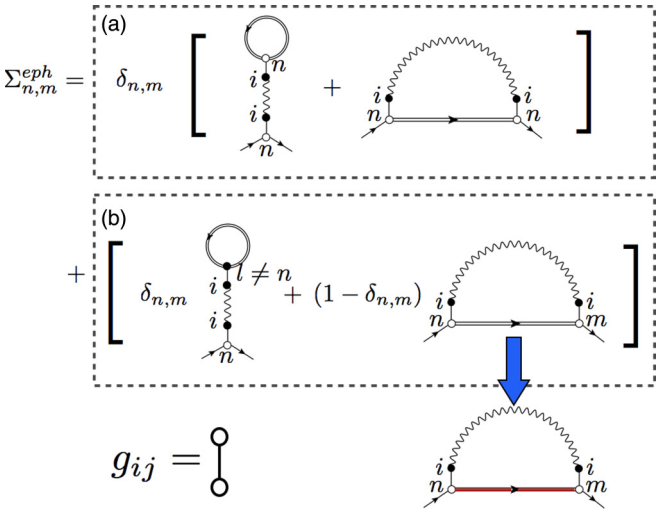

FIG. 1. (Color online) Electron-phonon interaction diagrams. The open straight line is the nonaveraged electron propagator, the filled straight line is the disorder-averaged electron propagator, and the wavy line is the phonon propagator.

propagator is not renormalized by the electron density fluctuations; we therefore associate the phonon frequency with that obtained by experiment, or we assume that the phonon frequency renormalization is negligible at low electron density.

After Matsubara's frequency summation, the PPNCA self-energy is written as

$$\hat{\Sigma}_{e\text{-ph}}(\omega) = g^2 \int d\epsilon \hat{A}(\epsilon) \left[\frac{b(\omega_0) + f(\epsilon)}{\omega + \omega_0 - \epsilon + \imath\delta} + \frac{b(\omega_0) + 1 - f(\epsilon)}{\omega - \omega_0 - \epsilon + \imath\delta} \right] + \hat{\Sigma}_H, \tag{13}$$

with $b(\omega_0)$ and $f(\epsilon)$ referring to the Bose-Einstein and Fermi-Dirac distributions, respectively, and $\hat{A}(\epsilon) = (-1/\pi)\text{Im}\hat{\mathcal{G}}(\epsilon)$ being the spectral function.

The averaged propagator is translationally invariant. It can be expressed in terms of the local self-energy as $G(k,\omega) = 1/[\omega - \epsilon_k - \Sigma(\omega)]$. The averaged local propagator is thus

$$G_{\text{loc}}(\omega) = \int d\epsilon N(\epsilon) \frac{1}{\omega - \epsilon - \Sigma(\omega)}, \tag{14}$$

where $N(\epsilon) = \sum_k \delta(\epsilon - \epsilon_k)$ is the noninteracting density of states. The self-consistency condition requires the single-site Green's function (10) to coincide with the local lattice Green's function (14),

$$G_{\text{loc}}(\omega) = \mathcal{G}(\omega). \tag{15}$$

In this way, Eqs. (9), (10), (13), (14), and (15) define a self-consistency loop to be iterated to get the self-consistent local self-energy, which takes into account disorder at the CPA level as well electron-phonon interaction coming only from diagrams of type (a) in Fig. 1. We call this scheme PPNCACPA. From the operative point of view, starting with an educated guess for G_0, we use Eqs. (10) and (13) to determine $\mathcal{G}$, Eq. (15) to obtain Σ, and Eq. (9) to obtain a new G_0 for iterating the

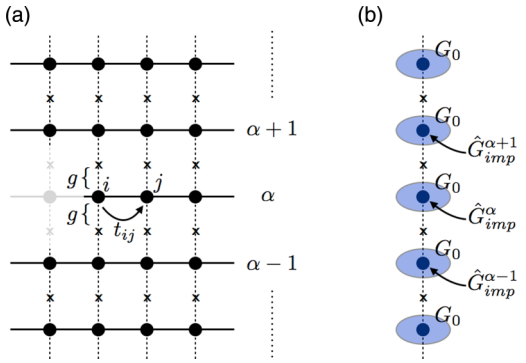

FIG. 2. (Color online) DMFT mapping of the AO model. (a) Lattice model in which electrons move on the planes and interact with the AO phonon. (b) Mapping of the lattice problem into a single-chain single-site model.

procedure. This iteration scheme differs from DMFT due to the approximate treatment of the electron-phonon interaction trough PPNCA.

B. PPNCACPA in the AO model

To generalize PPNCACPA to the AO model, we have to introduce the planar structure into our single-site model. We have a chain of single-site models as depicted in Fig. 2. The interaction between neighboring planes occurs through the electron-phonon interaction [see Eq. (8)]. In the AO model, we neglect the interplane hopping, and therefore the self-consistent G_0 is plane-diagonal. Equation (10) can be generalized as

$$\mathcal{G}(\omega)=\left[\frac{1}{G_0^{-1}(\omega)-\xi_\alpha-\hat{\Sigma}^{\alpha}_{e\text{-ph}}(\omega)}\right]_{\xi}, \tag{16}$$

where α is the plane index. Notice that after averaging, $\mathcal{G}$ does not depend on the plane indexes.

Now we have to generalize Eq. (13) to the BM model. Defining the upper and lower local phonon propagators as

$$D^{(\pm)}(t)=-i\langle T x_{i,\alpha\pm1/2}(t)x_{i,\alpha\pm1/2}(0)\rangle, \tag{17}$$

the Fock and Hartree terms of the electron-phonon self-energy take the form

$$\hat{\Sigma}^{\alpha}_{F}(\omega)=-\frac{g^2}{2\beta}\sum_m D^{+}(\omega-\imath\omega_m)\hat{\mathcal{G}}^{\alpha}(\imath\omega_m) -\frac{g^2}{2\beta}\sum_m D^{-}(\omega-\imath\omega_m)\hat{\mathcal{G}}^{\alpha}(\imath\omega_m), \tag{18}$$

$$\hat{\Sigma}^{\alpha}_{H}=\frac{g^2}{2}[D^{+}(0)\hat{n}^{\alpha}-D^{-}(0)\hat{n}^{\alpha+1}] +\frac{g^2}{2}[D^{+}(0)\hat{n}^{\alpha}-D^{-}(0)\hat{n}^{\alpha-1}], \tag{19}$$

where $D^{(\pm)}(\imath\omega_n)$ are the local phonon propagators in the Matsubara frequencies and $\hat{n}^{\alpha}=\frac{1}{\beta}\sum_n\hat{\mathcal{G}}^{\alpha}(\imath\omega_n)e^{i\omega_n0^+}$ is the local density on a generic site of the plane α. Notice that $\hat{n}^{\alpha}$ still depends on the disorder realization. Notice also that interplane coupling occurs due to the Hartree term in the self-energy Eq. (19). After Matsubara's frequency summation, the Fock contribution to the self-energy is written as

$$\hat{\Sigma}^{\alpha}_{F}(\omega)=g^2\int d\epsilon\,\hat{A}^{\alpha}(\epsilon)\left[\frac{b(\omega_0)+f(\epsilon)}{\omega+\omega_0-\epsilon+\imath\delta} +\frac{b(\omega_0)+1-f(\epsilon)}{\omega-\omega_0-\epsilon+\imath\delta}\right], \tag{20}$$

with $\hat{A}^{\alpha}(\epsilon)=(-1/\pi)\mathrm{Im}\hat{\mathcal{G}}^{\alpha}(\epsilon)$ being the αth plane spectral function. The scheme of iteration is basically the same as for the Holstein (LOC) model with an important difference: we have to iterate the self-consistency condition for an array of planes. Adopting periodic boundary conditions, we need 64 planes to achieve convergence for the sets of parameters used throughout the paper.

C. Generalization to nonlocal models of electron-phonon interaction

Now let us consider a general nonlocal electron-phonon interaction such as that of the model NLOC, Eq. (3). The perturbation theory in terms of the electron-phonon coupling constant $g_{i,j}$ can be written in the lattice space. This is shown diagrammatically in Fig. 1. The diagram sets are divided into two groups: (a) refers to local-type diagrams in which only the $[g^2]_{n,n}$ appears (see the discussion about the LOC model), while (b) contains extra terms that include $[g^2]_{n,m}$ for $m\neq n$. We divide our calculation into two steps.

In a first step, we implement the PPNCACPA previously described for the Holstein (LOC) model, taking into account the (a) diagrams for the electron-phonon interaction. We use in this stage a coupling constant $g^2=[g^2]_{i,i}$. Within such a treatment, we are taking into account disorder and electron-phonon interaction at the local level. Now we include the nonlocal part of electron-phonon interaction, including diagrams of type (b) *at the average level*, i.e., we consider the internal propagator averaged over disorder. Average restores translational invariance, and the Hartree term [the tadpole diagram in Fig. 1(b)], which is independent of frequency, can be reabsorbed in the definition of the chemical potential. The only relevant term is the Fock one averaged over disorder, as depicted in Fig. 1(b) and highlighted by the blue arrow. The self-energy thus takes into account both disorder and electron-phonon interaction, while disorder and the local part of the electron-phonon interactions [diagrams (a)] are evaluated self-consistently; the nonlocal part is taken into account non-self-consistently in a final stage. Therefore, this approach should not be extended to the polaronic type of couplings. However, due to the relevance of disorder in our calculations, we have checked that the results do not depend on the actual value of the screening wave vector provided that $\kappa>0.001$, and thus on the specific form of the nonlocal e-ph coupling.

D. Alternative CPA schemes

To investigate the correlations in the one-particle spectra between disorder and electron-phonon interaction, in the local PPNCACPA loop we can compare two CPA schemes: the one we are actually using, in which the electron-phonon self-energy depends on local random potentials (CPA2), and a

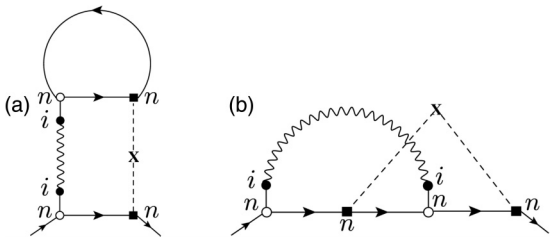

FIG. 3. Examples of diagrams neglected in the CPA1 scheme for Gaussian-distributed disorder. (a) A correction that takes into account disorder correlations in the Hartree part of the self-energy entering in Eq. (10) within the CPA2 scheme but neglected in the same expansion within the CPA1 scheme. The solid line represents the self-consistent propagator G_0, the wavy line the phonon propagator, and the dashed line disorder insertion. (b) A disorder-induced vertex correction appearing in the expansion of the Fock part of the local electron-phonon self-energy.

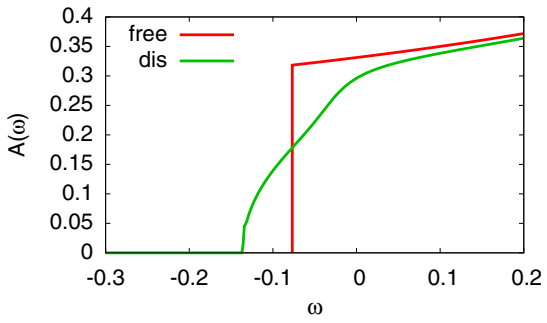

FIG. 4. (Color online) DOS, $A(\omega)$, of the noninteracting system (free) shifted to match the filling of the 5% doped system (dis). Unit of frequency is D; the zero of frequency is set to the chemical potential.

simpler scheme, in which we average the e-ph self-energy diagrams of type (a) on disorder (CPA1). In the case of NLOC models, to take into account the nonlocality of the electron-phonon interaction, we finally implement the second stage of our approximation having the local self-energy from CPA2 or CPA1 formulations. Notice that the CPA1 scheme, in the absence of electron-phonon interaction, is usually referred to as the *virtual-crystal* approximation [44]. The comparison between the two schemes still gives us an idea of the relevance of the electron-phonon self-energy fluctuations due to disorder at different energy scales.

We notice that averaging the internal propagators appearing in diagrams of type (a) shown in Fig. 1 means substituting the internal electron propagators with their averages. The Hartree contribution [the tadpole diagram in Fig. 1(a)] averages to a frequency and k-independent value, thus reducing to a mere shift of the chemical potential. The remaining contribution is the Fock term, in which the internal propagator has been averaged over disorder. This average procedure neglects (i) correlations between the density and the disorder variable at a given site, and (ii) disorder and electron-phonon correlated scatterings. From a perturbative point of view, the diagrams that contribute to these two mechanisms are depicted in Fig. 3.

We notice that, due to our strong-disorder approach, these contributions are not included in the self-consistent Born approximation approach of Ref. [27].

IV. RESULTS

Here we present results obtained using basically two kinds of disorder. We first consider a dichotomic disorder (P_i distribution) in which a percentage $x = 5\%$ of sites has a lower energy $E_b = -0.5$ (in units of the half-bandwidth) than all the other sites. This kind of disorder mimics the introduction of impurities associated with doping. Toward that end, we fix the filling factor to the same value x. We also consider Gaussian-uncorrelated disorder (P_g distribution), which can mimic a strong structural disorder, as usually happens in thin films. Even though 5% of impurities seems to be a rather small quantity, it can affect severely the lower part of the energy spectrum, as can be seen in Fig. 4. Moreover, this is precisely the energy range in which electron-phonon interaction is relevant ($\omega \simeq \omega_0$).

On top of this disordered system, we consider a weak electron-phonon interaction $\lambda = 0.22$, which is the same in all the considered models. To disentangle the separate action of electron-phonon interaction and disorder, we show the spectral function in the case of the LOC model in Fig. 5. There the spectral function is compared along a cut on the k_x axis around the Γ point in the presence of electron-phonon interaction only [panel (a)], in the presence of impurities without electron-phonon interaction [panel (b)], and under the action of both electron-phonon interaction and impurity disorder in panel (c). It is immediately seen that the spectra in panel (c) cannot be obtained by a simple broadening of the spectra of panel (a). A complete redistribution of the spectral weight is obtained under the action of a quite low electron-phonon coupling in the presence of disorder. The growing of an impurity band appears to be evident at the bottom of the coherent electronic band with a merging around the chemical potential. On the other hand, the action of such a strong disorder does not prevent the typical fingerprints of the electron-phonon interaction, such as the kinks at the phonon frequency (see Appendix A). This result highlights the fact that when disorder and electron-phonon coupling interact at the same energy scales, as in the considered case, the action of disorder cannot be taken into account as a simple broadening of the spectral features in the absence of disorder, since disorder and electron-phonon interaction work in a cooperative way.

In panel (d), we plot the spectra obtained using a Gaussian disorder with $\sigma^2 = 0.08$. We have chosen the variance of disorder requiring the same value of the Fermi k_F as that given by the 5% impurities. In this case, an energy-dependent broadening can be seen in the picture while the phonon signature, even weak, is still visible. Clearly the interplay of impurities and distributed Gaussian disorder with electron-phonon interaction is very different.

The scenario presented in Fig. 5 is rather general; indeed, it holds also in the case of highly nonlocal electron-phonon interaction. In Fig. 6, we have considered an electron-phonon interaction of the kind in Eq. (5) with the screening k vector $\kappa = 10^{-3}$. Comparing the spectra in the absence of disorder [Figs. 5(a) and 6(a)], we see that the enhanced forward scattering present in the NLOC model broadens the low-energy features around the Γ point. However, in the presence of

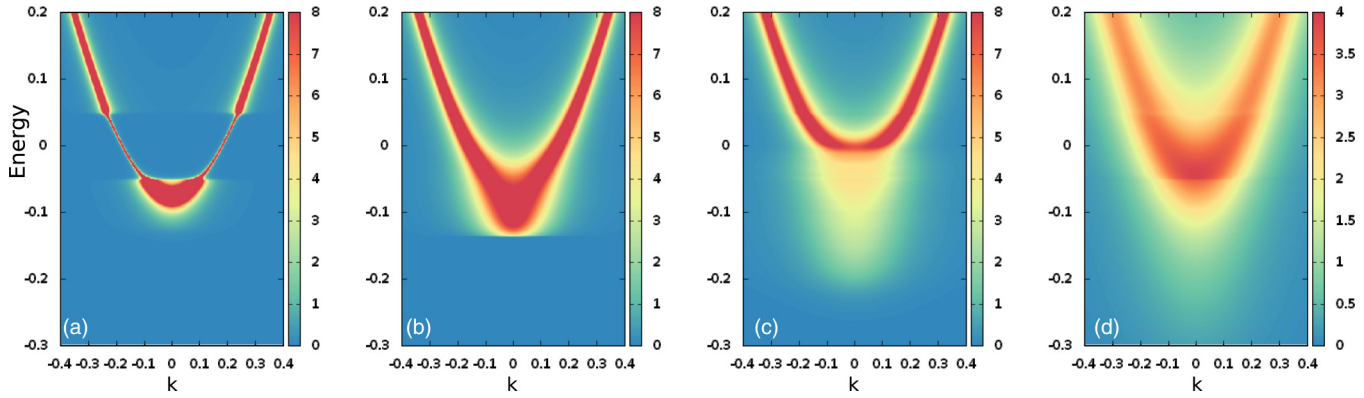

FIG. 5. (Color online) The spectral function $A(k,\omega)$ for the LOC model. (a) Electron-phonon interaction only, $\lambda = 0.22$. (b) Disorder only. (c) Electron-phonon interaction + disorder. (d) Electron-phonon interaction + Gaussian disorder; the color map (range of z) has been expanded in this case to take into account the lower value of the spectral function.

impurities [Figs. 5(c) and 6(b)], the spectra look much more similar even if phonon signatures are more marked in the NLOC model. This is consistent with the relevance of such a strong disorder at the highest binding energies. Increasing the screening, the range of electron-phonon interaction decreases, and the qualitative scenario becomes increasingly similar to that of the LOC model. With the chosen values of parameters at $\kappa = 10^{-2}$, the spectra are almost indistinguishable from those of Fig. 5.

A quantitative measure of the interplay between electron-phonon and disorder effects can be probed by measuring the deviation of the Fermi wave vector (k_F) from that predicted by Luttinger's theorem [45] at a given electron density. In Fig. 7 (upper panel), the momentum distribution curve (MDC) is obtained from the spectral function. Luttinger's prediction for k_F coincides with the position of the peaks in the presence of electron-phonon interaction only. Indeed, in this case the damping at the Fermi energy is zero and the Fermi surface area is conserved; thus the sole presence of electron-phonon interaction does not lead to a Fermi vector reduction. Disorder alone, even when strong as in our case, contributes to a decrease of k_F only by 10%, while the additional presence of a relatively weak electron-phonon interaction dramatically reduces k_F by 60%. If one takes Luttinger's theorem [45] for granted in these conditions, the obtained electron density is far from the nominal one given by the impurities' concentration. This evidence should be carefully taken into account for the interpretation of experimental ARPES spectra, being the fingerprint of a strong interplay between disorder and electron-phonon interaction [14]. In the lower panel of Fig. 7, a comparison is shown of the MDC curves for the LOC, NLOC, and AO models. We see that the reduction of k_F is less effective

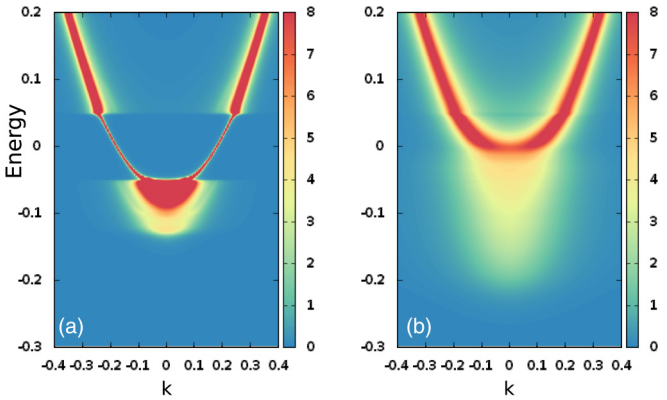

FIG. 6. (Color online) The spectral function $A(k,\omega)$ for the NLOC model. (a) Electron-phonon interaction only, $\lambda = 0.22$. (b) Electron-phonon interaction + disorder.

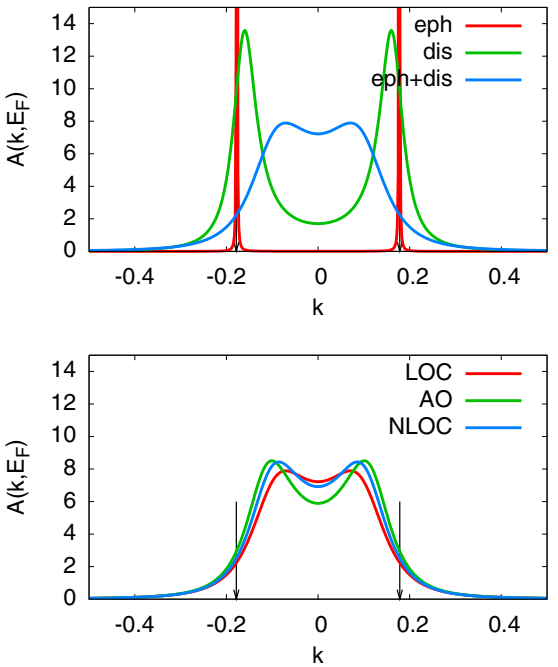

FIG. 7. (Color online) Upper panel: an MDC scan at Fermi energy in the LOC model. (e-ph) stands for the nondisordered system under the action of electron-phonon interaction only. (dis) is the purely disordered system without electron-phonon interaction. (e-ph+dis) is the system under the action of both electron-phonon and disorder. Lower panel: an MDC scan at Fermi energy in the LOC compared with the NLOC and AO model for the same value of electron-phonon coupling, $\lambda = 0.22$, and the same disorder variables $x = 0.05, E_b = -0.5$. Vertical arrows mark Luttinger's theorem value for k_F.

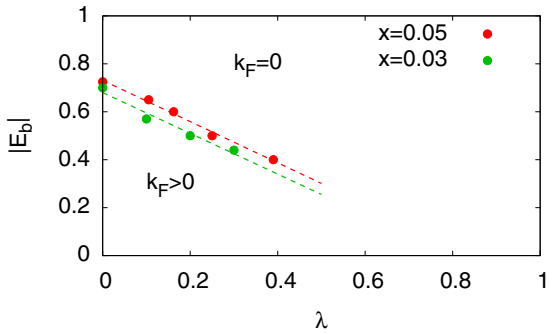

FIG. 8. (Color online) The phase diagram of the LOC model at zero temperature for $x = 0.03$ and 0.05. Points are obtained at values of parameters such that $k_F = 0$. Dashed lines are linear fits of the data. At a given value of λ, the increase of impurity concentration stabilizes the conductive phase.

in the NLOC and AO models compared to the LOC one. We will discuss the reason for this behavior below.

The cooperative action of electron-phonon and disorder interactions is particularly evident in the disorder-induced metal-insulator transition that occurs as a function of the electron-phonon coupling λ. In this work, the disorder-induced MIT is defined looking at the vanishing of the Fermi vector k_F. A vanishing k_F is a precursor of a vanishing density of states at the Fermi level, which in turn leads to an insulating state. It is well known that, in a disordered system, increasing the binding energy of the impurities will produce a metal-insulator transition in which an impurity band detaches from the conduction band [46]. Here we achieve the same phenomenon using the synergistic action of electron-phonon interaction, as is shown in Fig. 8 for two different impurity concentrations.

For a given value of $E_b = -0.5$, we report the density of states (DOS), which clearly opens a gap at $\lambda = 0.275$ in Fig. 9 (upper panel). The vanishing of the Fermi surface occurs at a lower value of λ, as is shown in the inset of the same figure. The synergistic work of electron-phonon interaction originates from the action of the Hartree term, Eq. (12), which provides an electron-phonon-induced increase of the binding energy which is proportional to the carrier density at a given site. This is correlated with the presence of the impurity since the density will be higher just at the impurity sites (see Appendix B). When the electron-phonon interaction is nonlocal, this effect is less marked, as can be seen in Fig. 9 (lower panel). For instance, in the AO model, as the Hartree energy Eq. (18) does depend on the density on nearest-neighbor planes along the chain, the interplay between electron-phonon interaction and disorder is less effective, as seen also in the smaller reduction of the Fermi surface with respect to the LOC model (see Fig. 7, lower panel).

Moreover, a further insight into the interplay between electron-phonon and disorder interaction can be obtained by the comparison of our results within the two CPA schemes (see Sec. III). The DOSs and the spectra obtained by CPA1 and CPA2 are compared in Fig. 10 (upper and lower panels, respectively). We see how the interplay between *e*-ph interaction and disorder affects the DOS below the Fermi energy, just in the energy region in which both disorder and

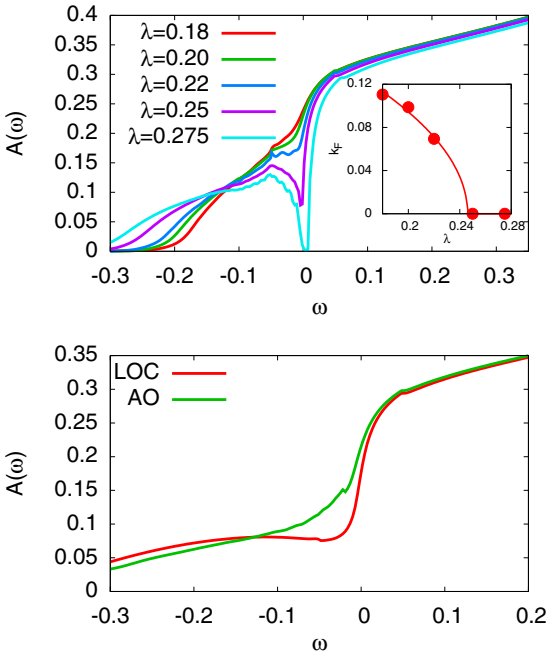

FIG. 9. (Color online) Upper panel: the interacting density of the states for $x = 0.05$ and disorder level $E_b = -0.5$ as a function of electron-phonon coupling λ. In the inset is shown the value of k_F as a function of λ. Lower panel: The DOS of the LOC and AO models at $\lambda = 0.3$; here a Gaussian disorder of std. deviation $\sigma = 0.05$ has been added to the dichotomic disorder.

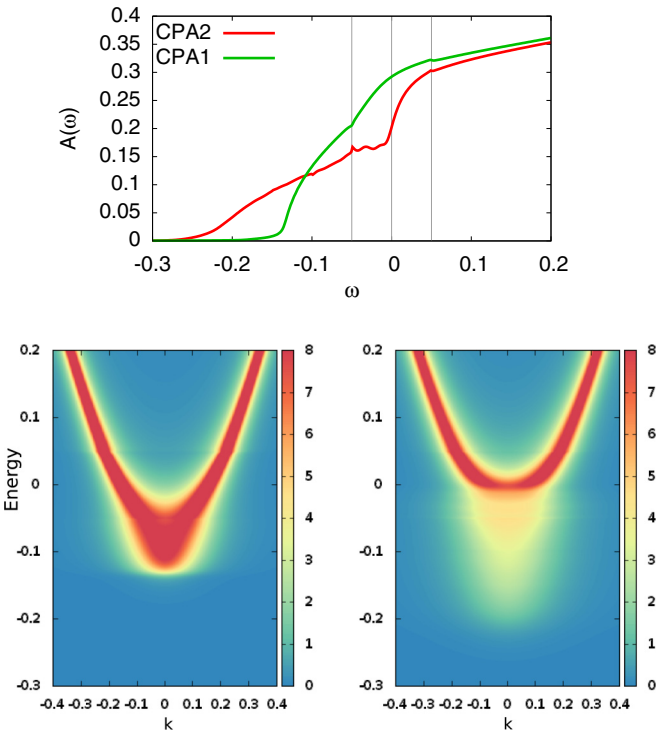

FIG. 10. (Color online) Upper panel: DOS of the LOC model within CPA1 and CPA2 approximations; vertical dotted lines marks the Fermi energy ($\omega = 0$) and the two-phonon resonances at $\pm\omega_0$. Lower panel: Comparison of CPA1 (left) and CPA2 (right) spectra.

e-ph are present. Noticeably, phonon signatures appear much more evident in the CPA2 scheme, and a large spectral weight redistribution occurs at higher binding energies. Moreover, we see that within the CPA1 scheme the effect of disorder is largely dominant, as can be seen by comparing the spectrum of Fig. 10 (lower left panel) and that obtained in the presence of pure disorder [see Fig. 5(c)]. Since in CPA1 we average the electron-phonon self-energy over the disorder variable, we can ascribe the large discrepancies between the spectra in Fig. 10 to the correlation between electron-phonon and disorder effects in the self-energy. This issue can be analyzed from the point of view of perturbative expansions. The resummation in the CPA2 scheme of diagrams of type (a) in Fig. 3, which take into account the correlation at the Hartree level between electron-phonon and local disorder, leads to an enhancement of the electron-phonon interaction effects on the energy scale of the emerging impurity band (around $\simeq E_b$ from the Fermi level). In contrast to CPA1, the CPA2 Hartree term is correlated to the presence of the impurity leading to the λ dependence of the disorder-induced metal-insulator transition (see the discussion above and the upper panel of Fig. 9). For this reason, as shown in Fig. 10, the impurity band within CPA2 seems to be more marked than that in CPA1. However, another aspect is clear from the comparison in Fig. 10: the CPA2 impurity band is also much wider than that obtained within CPA1, and, despite the strong disorder, prominent phonon signatures are still evident on the impurity band. This should be ascribed to the correlation between disorder and electron-phonon self-energy at the Fock level diagrams of type (b) in Fig. 3. In previous work, an interplay between the electron-phonon interaction and disorder has been found within the self-consistent Born approximation [27–29] in which, despite the self-energy separating into electron-phonon and disorder parts, nonadditivity in the electron-scattering time is found due to the self-consistency condition. We remark here on the difference in our strong-disorder approach in which the self-energy appearing in Eq. (14) is no longer separable into two contributions. We thus have analyzed the strong fluctuations of the self-energy due to disorder rather than its separability into electron-phonon and disorder parts.

V. CONCLUSIONS

In conclusion, in this work we have investigated the role of the electron-phonon interaction in disordered systems, and their strong interplay when the energy scales in which they act are comparable. It is well known that trapping impurities provide the necessary energy for the polaronic transition localizing the polaronic state at weaker electron-phonon coupling [23–26]. Here we have discussed this interplay at finite electron density and weak electron-phonon coupling, thus relying in our study on the PPNCA to deal with weak electron-phonon interaction. We have developed a theoretical method to combine the PPNCA with the CPA to study strongly disordered systems, and we have extended that theory to the apical oxygens model [38] and to a nonlocal electron-phonon interaction characteristic of couplings with a crystal's polar modes. We focused our attention mainly on low-dimensional systems such as quasi-two-dimensional or layered ones, since in these cases the effect of disorder can in principle be larger with respect to purely 3D systems. On the other hand, we concentrated on low-doped systems in which the impurity band can be very close to, and hybridizes with, the bottom of the electronic one. This peculiar but quite common experimental and theoretical evidence [7–9,14–17] allowed us to study when disorder and electron-phonon interaction act in a cooperative way, and the action of disorder cannot be included in a perturbative way as a source of weak broadening of the spectral features. On the contrary, impurity-type disorder strongly affects the electronic structure giving rise to a significant spectral weight redistribution. This could lead to a dramatic Fermi surface reduction even at moderate electron-phonon couplings, which in turn can be detected as a Luttinger's theorem violation [14] and eventually an electron-phonon driven metal-insulator transition as the Fermi surface vanishes. From a quantitative point of view, the strongest interplay between electron-phonon and local disorder is found for the local electron-phonon interaction (LOC model). Nonlocal couplings studied in this work (AO, NLOC) both display a less effective interplay with disorder as a consequence of the interactions' nonlocality.

The CPA used to approach the strong disorder regime is a reasonable approximation for the DOS or the average spectral function in three dimensions [47]. In our 2D (LOC,NLOC) or (2+1) (AO) -dimensional systems, there are, however, some deviations that can be treated within a nonlocal DCA framework [48]. Generally speaking, the CPA overestimates the disorder-induced gap. Going beyond the CPA, we expect that the binding energy E_b needed to reach the MIT would be slightly higher. Localization effects, absent in the CPA approach, which are, however, beyond the present work, can be relevant for transport properties in low-dimensional systems. Their effects can be probed at the local level by anomalous fluctuations of the local DOSs, which can be relevant to tunneling experiments. Instead of the averaged DOS taken into account in this work, one can consider the typical DOS obtained as geometric averages of local DOSs [47]. As far as local quantities are concerned, for the LOC model one can generalize our self-consistency equations to the case of typical quantities following along the lines of Refs. [47,49].

The PPNCA for the electron-phonon interaction used in our work cannot be used to attack the polaronic regime, which can be interesting to study, because of the recently found polaronic resonances in single-layer high-T_c superconducting FeSe [10]. Also from a theoretical point of view, the interplay between disorder and polaronic electron-phonon interaction could be much different from that proposed in the present paper [38]. Toward that end, a beyond-NCA approach such as DMFT should be useful also to include electronic correlations. A cluster-DMFT approach could also be useful to include spatial correlations, which we neglect in our local approach in the LOC model case, overcoming in this way the well-known problems of single-site DMFT in dealing with systems at low dimensionality [50].

ACKNOWLEDGMENTS

The authors kindly thank K. Shen and Y. Nie for very helpful discussions and hints on the work. Helpful discussions with E. Cappelluti, P. Barone, G. Sangiovanni, and R. Valentí are

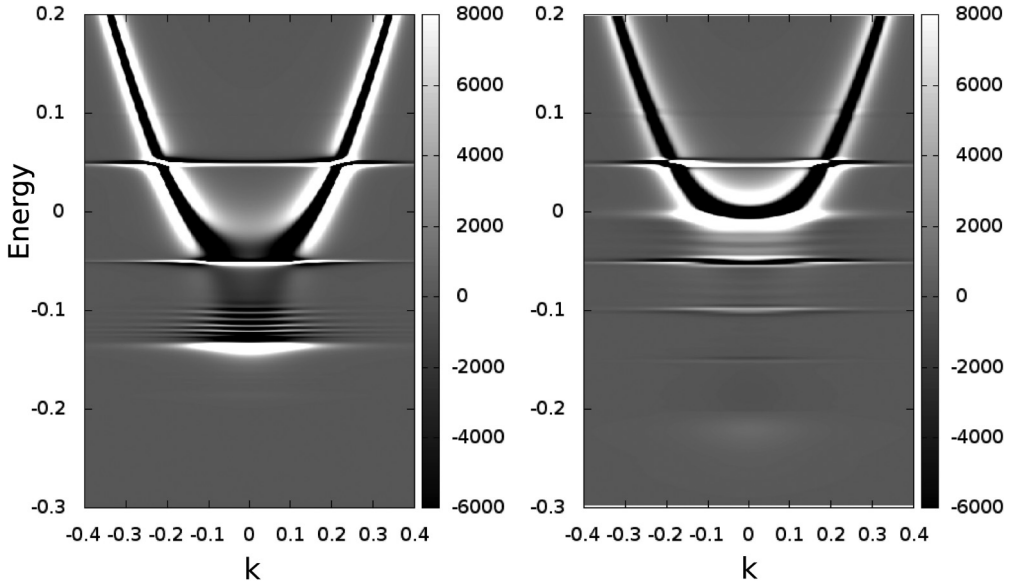

FIG. 11. Comparison of the second derivative of the spectral function within CPA1 (left) and CPA2 (right) spectra.

also acknowledged. The computational support from the CINECA supercomputing center under the grant "ConvR_aq_caspF" is gratefully acknowledged. The authors acknowledge funding from project PRIN No. 2012X3YFZ2_006.

APPENDIX A: SECOND DERIVATIVE OF THE SPECTRAL FUNCTION

A commonly used technique to highlight subtle spectral features is to take the second derivative of the spectral function $\frac{\partial^2}{\partial\omega^2}A(\mathbf{k},\omega)$. In Fig. 11, we plot this function using CPA1 and CPA2 iteration schemes. In both cases, the phonon's signatures are evident but a little bit more within CPA2. More importantly, at higher binding energies, CPA1 spectra clearly show disorder nondispersed features, while in CPA2 the phonon's higher-order resonances are clearly visible up to fourth order, even in the presence of such a strong disorder.

APPENDIX B: ELECTRON-PHONON INDUCED MOTT TRANSITION

Let us consider the bimodal disorder case $P_i(\xi) = x\delta(\xi - E_b) + (1-x)\delta(\xi)$ in the LOC model. Let us consider only the action of the Hartree term in the self-energy, Eq. (12), so that the single-site Green function [Eq. (10)] reads

$$\mathcal{G}(\omega) = \frac{x}{G_0^{-1}(\omega) - E_b + \lambda n_1} + \frac{1-x}{G_0^{-1}(\omega) + \lambda n_0}, \tag{B1}$$

where

$$n_1 = \frac{1}{\beta}\sum_n \frac{x}{G_0^{-1}(\omega) - E_b + \lambda n_1} e^{i\omega_n 0^+}, \tag{B2}$$

$$n_0 = \frac{1}{\beta}\sum_n \frac{1-x}{G_0^{-1}(\omega) + \lambda n_0} e^{i\omega_n 0^+}, \tag{B3}$$

where n_1 is the electron density in the impurity site and n_0 is the density everywhere else. In the atomic (zero hopping) limit, we have $n_1 = 1$ and $n_0 = 0$, but due to the hybridization of the impurity sites, $n_1 < 1$ and $n_0 > 0$. From Eqs. (B1)–(B3) it is evident that as far as the electron-phonon interaction is concerned, at the Hartree level $E_b \to E_b - \lambda(n_1 - n_0)$ and the disorder-induced metal-insulator transition occurs when

$$|E_b| = |E_{\mathrm{MIT}}| - \lambda(n_1 - n_0), \tag{B4}$$

with $|E_{\mathrm{MIT}}|$ the binding energy at the impurity site needed to detach the impurity band in the absence of electron-phonon interaction. Equation (B4) explains the linear dependence found for small λ for the disorder-induced metal-insulator transition in Fig. 8. It is worth noting that this effect is absent in CPA1, where the electron-phonon self-energy is mediated and as a consequence there is no electron-phonon contribution to the binding energy at the impurity site.

[1] A. Damascelli, Z. Hussain, and Z. X. Shen, Rev. Mod. Phys. **75**, 473 (2003).
[2] T. Cuk, D. H. Lu, X. J. Zhou, Z.-X. Shen, T. P. Devereaux, and N. Nagaosa, Phys. Status Solidi B **242**, 11 (2005).
[3] E. Dagotto, T. Hotta, and A. Moreo, Phys. Rep. **334**, 1 (2001).
[4] Y. Tokura, Phys. Today **56**(7), 50 (2003).
[5] M. Z. Hasan and C. L. Kane, Rev. Mod. Phys. **82**, 3045 (2010).
[6] A. H. Castro Neto, F. Guinea, N. M. R. Peres, K. S. Novoselov, and A. K. Geim, Rev. Mod. Phys. **81**, 109 (2009).

[7] Y. J. Chang, A. Bostwick, Y. S. Kim, K. Horn, and E. Rotenberg, Phys. Rev. B **81**, 235109 (2010).

[8] W. Meevasana, X. J. Zhou, B. Moritz, C.-C. Chen, R. H. He, S.-I. Fujimori, D. H. Lu, S.-K. Mo, R. G. Moore, F. Baumberger, T. P. Devereaux, D. van der Marel, N. Nagaosa, J. Zaanen, and Z.-X. Shen, New J. Phys. **12**, 023004 (2010).

[9] M. Takizawa, K. Maekawa, H. Wadati, T. Yoshida, A. Fujimori, H. Kumigashira, and M. Oshima, Phys. Rev. B **79**, 113103 (2009).

[10] J. J. Lee, F. T. Schmitt, R. G. Moore, S. Johnston, Y.-T. Cui, W. Li, M. Yi, Z. K. Liu, M. Hashimoto, Y. Zhang, D. H. Lu, T. P. Devereaux, D. -H. Lee, and Z.-X. Shen, arXiv:1312.2633.

[11] S. Moser, L. Moreschini, J. Jaćimović, O. S. Barišić, H. Berger, A. Magrez, Y. J. Chang, K. S. Kim, A. Bostwick, E. Rotenberg, L. Forró, and M. Grioni, Phys. Rev. Lett. **110**, 196403 (2013).

[12] R. Nourafkan, F. Marsiglio, and G. Kotliar, Phys. Rev. Lett. **109**, 017001 (2012).

[13] T. Kondo, Y. Nakashima, Y. Ota, Y. Ishida, W. Malaeb, K. Okazaki, S. Shin, M. Kriener, S. Sasaki, K. Segawa, and Y. Ando, Phys. Rev. Lett. **110**, 217601 (2013).

[14] Y. F. Nie, D. Di Sante, S. Chatterjee, P. D. C. King, M. Uchida, S. Ciuchi, D. G. Schlom, and K. M. Shen (unpublished).

[15] P. Richard, T. Sato, S. Souma, K. Nakayama, H. W. Liu, K. Iwaya, T. Hitosugi, H. Aida, H. Ding, and T. Takahashi, Appl. Phys. Lett. **101**, 232105 (2012).

[16] J. Okabayashi, A. Kimura, O. Rader, T. Mizokawa, A. Fujimori, T. Hayashi, and M. Tanaka, Phys. Rev. B **64**, 125304 (2001).

[17] M. A. Majidi, J. Moreno, M. Jarrell, R. S. Fishman, and K. Aryanpour, Phys. Rev. B **74**, 115205 (2006).

[18] G. Berner, M. Sing, H. Fujiwara, A. Yasui, Y. Saitoh, A. Yamasaki, Y. Nishitani, A. Sekiyama, N. Pavlenko, T. Kopp, C. Richter, J. Mannhart, S. Suga, and R. Claessen, Phys. Rev. Lett. **110**, 247601 (2013).

[19] A. F. Santander-Syro, O. Copie, T. Kondo, F. Fortuna, S. Pailhés, R. Weht, X. G. Qiu, F. Bertran, A. Nicolaou, A. Taleb-Ibrahimi, P. Le Févre, G. Herranz, M. Bibes, N. Reyren, Y. Apertet, P. Lecoeur, A. Barthélémy, and M. J. Rozenberg, Nature (London) **469**, 189 (2011).

[20] J. Shen, H. Lee, R. Valentí, and H. O. Jeschke, Phys. Rev. B **86**, 195119 (2012).

[21] N. Reyren, S. Thiel, A. D. Caviglia, L. Fitting Kourkoutis, G. Hammerl, C. Richter, C. W. Schneider, T. Kopp, A.-S. Rüetschi, D. Jaccard, M. Gabay, D. A. Muller, J.-M. Triscone, and J. Mannhart, Science **317**, 1196 (2007).

[22] A. N. Das and S. Sil, Phys. Lett. A **348**, 266 (2006).

[23] J. P. Hague, P. E. Kornilovitch, and A. S. Alexandrov, Phys. Rev. B **78**, 092302 (2008).

[24] M. Berciu, A. S. Mishchenko, and N. Nagaosa, Europhys. Lett. **89**, 37007 (2010).

[25] C. A. Perroni and V. Cataudella, Phys. Rev. B **85**, 155205 (2012).

[26] H. Ebrahimnejad and M. Berciu, Phys. Rev. B **85**, 165117 (2012).

[27] E. Cappelluti and L. Pietronero, Phys. Rev. B **68**, 224511 (2003).

[28] A. Knigavko and J. P. Carbotte, Phys. Rev. B **73**, 125114 (2006).

[29] F. Dogan and F. Marsiglio, J. Sup. Nov. Magn. **20**, 225 (2007).

[30] A. Chen, G. Weisz, and A. Scher, Phys. Rev. B **5**, 2897 (1972).

[31] S. M. Girvin and M. Jonson, Phys. Rev. B **22**, 3583 (1980).

[32] B. M. Letfulov and J. K. Freericks, Phys. Rev. B **66**, 033102 (2002).

[33] J. K. Freericks and V. Zlatić, Rev. Mod. Phys. **75**, 1333 (2003).

[34] It is worth noting that even a modest amount of impurities can introduce strong disorder effects at the energy scale of the order of the impurities' binding energy.

[35] S. Das Sarma and B. A. Mason, Ann. Phys. (NY) **163**, 78 (1985).

[36] Our definition of λ comes from the Eliashberg theory [G. M. Eliashberg, Sov. Phys. JETP **11**, 696 (1960)], for the Holstein model, applied to a spin-degenerate (band filling 2) squared density of states, a good approximation for a 2D DOS at very low density, around the band's bottom. We can write $\lambda = 2\int_0^\infty d\omega\, \alpha^2F(\omega)/\omega = 2\int_0^\infty d\omega\, N_0 g^2 \delta(\omega - \omega_0)/\omega = 2g^2N_0/\omega_0$, where $N_0 = 1/D$ is the density of states at the Fermi level, and D is the half-bandwidth.

[37] O. Gunnarsson and O. Rösch, J. Phys.: Condens. Matter **20**, 043201 (2008).

[38] B. Lau, M. Berciu, and G. A. Sawatzky, Phys. Rev. B **76**, 174305 (2007).

[39] L. Schwartz and E. Siggia, Phys. Rev. B **5**, 383 (1972).

[40] D. Vollhardt, in *Correlated Electron Systems*, edited by V. J. Emery (World Scientific, Singapore, 1992).

[41] A. Georges, G. Kotliar, W. Krauth, and M. J. Rozenberg, Rev. Mod. Phys. **68**, 13 (1996).

[42] F. X. Bronold, A. Saxena, and A. R. Bishop, Phys. Rev. B **63**, 235109 (2001).

[43] To avoid confusion with the acronym NCA used in the theory of strongly correlated electrons system, we name our approximation PPNCA to indicate a theory that includes all noncrossing diagrams with respect to the phonon propagator. Notice that our theory includes diagrams in which disorder insertions cross with phonon propagators (see Fig. 3).

[44] D. Stroud and H. Ehrenreich, Phys. Rev. B **2**, 3197 (1970).

[45] In two dimensions, for a circular Fermi surface, the expression for k_F is $k_F = \sqrt{2x/\pi}$ [in units of (π/a)].

[46] With our choice of DOS at $x = 0.05$, the CPA gives $E_b = -0.725$ for the disorder-induced Mott transition.

[47] V. Dobrosavljević, A. A. Pastor, and B. K. Nikolić, Europhys. Lett. **62**, 76 (2003).

[48] M. Jarrell and H. R. Krishnamurthy, Phys. Rev. B **63**, 125102 (2001).

[49] H. Fehske, F.-X. Bronold, and A. Alvermann, in *Proceedings of the International School of Physics "Enrico Fermi," Course CLXI, Polarons in Bulk Materials and Systems with Reduced Dimensionality*, edited by G. Iadonisi, J. Ranninger, and G. de Filippis (IOS, Amsterdam, 2006), p. 313; F.-X. Bronold, A. Alvermann, and H. Fehske, Philos. Mag. **84**, 673 (2004).

[50] T. Maier, M. Jarrell, T. Pruschke, and M. Hettler, Rev. Mod. Phys. **77**, 1027 (2005).